Research Article

Methods in the Applied Sciences

Received 3 December 2016

Published online in Wiley Online Library

(wileyonlinelibrary.com) DOI: 10.1002/mma.4433
MOS subject classification: 76W05; 76D10; 65N06; 65H10

# Numerical and asymptotic study of non-axisymmetric magnetohydrodynamic boundary layer stagnation-point flows

**Ramesh B. Kudenatti**[a*†] **and Shreenivas R. Kirsur**[b]

**Communicated by D. Zeidan**

**Both numerical and asymptotic analyses are performed to study the similarity solutions of three-dimensional boundary-layer viscous stagnation point flow in the presence of a uniform magnetic field. The three-dimensional boundary-layer is analyzed in a non-axisymmetric stagnation point flow, in which the flow is developed because of influence of both applied magnetic field and external mainstream flow. Two approaches for the governing equations are employed: the Keller-box numerical simulations solving full nonlinear coupled system and a corresponding linearized system that is obtained under a far-field behavior and in the limit of large shear-to-strain-rate parameter ($\lambda$). From these two approaches, the flow phenomena reveals a rich structure of new family of solutions for various values of the magnetic number and $\lambda$. The various results for the wall stresses and the displacement thicknesses are presented along with some velocity profiles in both directions. The analysis discovered that the flow separation occurs in the secondary flow direction in the absence of magnetic field, and the flow separation disappears when the applied magnetic field is increased. The flow field is divided into a near-field (due to viscous forces) and far-field (due to mainstream flows), and the velocity profiles form because of an interaction between two regions. The magnetic field plays an important role in reducing the thickness of the boundary-layer. A physical explanation for all observed phenomena is discussed.** 

**Keywords:** MHD; shear-to-strain-rate; Keller-box; asymptotics

## 1. Introduction

Three-dimensional boundary-layer flow, in principle, has generated an increasing attention during recent years. Most of the studies on boundary-layer theory have been confined only to two-dimensional investigations because of the lack of rigorous mathematical tools to understand three-dimensional boundary-layer structures, and also, we see that the flow phenomena around us is in two-dimensional projection. Lack of accurate results also hampers efforts to comprehend important flow mechanisms, although these two-dimensional investigations proved to be a good starting point for identifying and understanding physical mechanisms and constructive features of three-dimensional boundary-layer flow. Because of the development of computers and rigorous mathematical tools, many studies have been undertaken on three-dimensional boundary-layer flow, and also because of applications of three-dimensional boundary-layer in different areas of engineering sciences, biomedical engineering, and industries. Of particular examples, boundary-layer over swept wings, turbine bodies, or a flying ball, etc. However, the three-dimensional boundary-layer flows still face a significant computational challenge, but when the solutions exist, they certainly predict interesting flow behavior and mechanisms. The complications in three-dimensional boundary-layer are

(i) an additional flow direction and hence an extra equation in the boundary layer equations;
(ii) two velocity components;
(iii) existence of secondary flow (i.e., flow inside and outside the boundary layer is not in the same direction); and
(iv) difficult to satisfy the boundary conditions (especially on the surface).

[a] *Department of Mathematics, Bangalore University, Central College Campus, Bangalore 560 001, India*
[b] *Department of Mathematics, Gogte Institute of Technology, Belagavi 560 008, India*
* *Correspondence to: Ramesh B. Kudenatti, Department of Mathematics, Bangalore University, Central College Campus, Bangalore 560 001, India.*
† *E-mail: ramesh@bub.ernet.in*

Simulations of the three-dimensional boundary-layer equations governed by a set of nonlinear partial differential equations will be required to provide the direct comparisons with many of the naturally observed phenomena. Because huge computational resources are required to simulate the three-dimensional boundary-layer flow, it is advisable to use the similarity transformations to convert these equations into a solvable system of nonlinear ordinary differential equations (in fact highly nonlinear), in a similar manner as that of well-versed two-dimensional boundary layer equations. Although a general treatment of the three-dimensional flow problem is extremely difficult because of the coupled equations, an approximate solution of the three-dimensional boundary-layer flow by momentum integral method has been given by Timman [1]. But this theory does not give satisfactory velocity distributions that leads to solution of three-dimensional boundary layer equations numerically, which was given by Howarth [2], Sears [3], and Carrier [4]. The finite difference method for incompressible three-dimensional boundary layer equations for blunt body has been given by Blottner [5]. The three-dimensional equations have been replaced by a nonlinear finite-difference equations and are solved using linearization. Solution have been obtained and compared with the several special cases. Nickel and Kirchgssner [6] have used many Crocco-type transformations to reduce the three-dimensional boundary-layer equations to a system of parabolic equations. Cousteix [7] has discussed the unsteady three-dimensional incompressible boundary-layer flow that has been developed under the influence of unsteadiness and given numerical computation of these equations.

In the aforementioned applications, the effect of applied magnetic field is not considered; however, on the other hand, magnetohydrodynamic (MHD) flows are considered to play a vital role in industrial applications, for example, in power generators, pumps, and polymer industry. For details, see [8]. It is widely known that applied magnetic field makes the viscous forces to confine to vicinity of the wall. That is to say that magnetic field releases more energy to the system that drives fluid faster, thereby increasing the Reynolds number. Along with this, the boundary-layer thickness also becomes thinner and thinner for increasing MHD. As in case of two-dimensional boundary-layer flows, the flow separation in the boundary-layer for adverse pressure gradient can be delayed by applying an external magnetic field. Takhar *et al*. [9] have given an unsteady three-dimensional boundary-layer flow of an incompressible viscous electrically conducting fluid. The governing partial differential equations have been solved by using an implicit finite difference scheme and discussed the effects of magnetic field and showed that the surface shear stresses increase with the magnetic field. Borelli *et al*. [10] have explained the effects of applied magnetic field in three-dimensional stagnation point flow of micropolar fluids and showed that magnetic field prevents the occurrence of the boundary-layer separation and reverse microrotation set-up by the micropolar fluid. Abdou and Soliman [11] have made an analysis on MHD boundary-layer flow of non-Newtonian viscoelastic fluid over a stretching surface and used recently developed homotopy analysis method for the analyses.

The motivation in the present study is to systematically investigate the effects of MHD on the three-dimensional non-axisymmetric stagnation point boundary-layer flow of Homann [12] where the outer potential flow is an irrotational. In the absence of MHD, Hewitt *et al*. [13] have considered a steady boundary-layer flow in a rotating cone in which the plate and fluid rotate at angular velocities $\omega$ and $\omega'$, respectively, and found that solutions to the Navier–Stokes equations in a small region. Recently, Weidman [14] has studied non-axisymmetric Homann's stagnation-point flows by adding radial and azimuthal velocities that leads to a new family of asymmetric viscous stagnation point flow governed by the shear-to-strain-rate parameter. We continue to pursue his study by applying an external magnetic field on the three-dimensional Homann's flow.

To determine the required flow phenomena, we need three-dimensional boundary-layer equations modified by the MHD, the Maxwell's and Ohm's law equations. These equations are then reduced to nonlinear ordinary differential equations using similarity transformations and solved for. The system is systematically solved for the velocity profiles, wall shear stresses, and displacement thicknesses for various physical parameters (i.e., the shear-to-strain-rate parameter $\lambda$ and Hartmann number $M$; these will be defined later). In this approach, the finite difference-based Keller-box method combined with LU decomposition is employed. The asymptotic approach for these equations for far-field behavior and for large $\lambda$ that has not been used in this context before is used.

The steady three-dimensional laminar incompressible viscous boundary-layer flow of an electrically conducting fluid has been studied. Presentation of the paper proceeds as follows. In Section 2, the three-dimensional boundary layer equations have been given, and transformed nonlinear ordinary differential equations have been given. The Keller-box method for the coupled system is provided in this section. In Section 3, the asymptotic solutions have been given for large $\lambda$ and far-field behavior. The linearized governing equations have been solved in terms of confluent hypergeometric functions and are given in Section 3. Important results are presented in Section 4 along with detailed physical reasons. Section 5 concludes the main findings of the three-dimensional boundary-layer problem.

## 2. Formulation of the problem

Following Rosenhead [15], we consider the incompressible laminar three-dimensional boundary-layer viscous flow over a wedge surface in an electrically conducting fluid. Let $x$-axis and $y$-axis be measured along the direction of the flow and $z$-axis be measured normal to the flow (Figure 1). Let $u$, $v$, and $w$ be the velocity components in $x$, $y$, and $z$-directions, respectively, and the flow occupies in the half space $z > 0$. It is assumed that the wedge surface is at rest and impermeable. Electrically conducting fluid of kinematic viscosity $\nu$ and constant density $\rho$ is considered. The magnetic field is applied normal to the flow. It is assumed that the magnetic Reynolds number is too small so that the induced magnetic field is negligible. Strength of electric field due to polarization of charges is also negligible. Fluid is moving with the potential velocities $U = U(x) = (a + b)x$ and $V = V(y) = (a - b)y$ along $x$-direction and $y$-direction, where $a$ and $b$ are strain and shear rates of stagnation point flow. Under these approximations, the Navier–Stokes equations for MHD are given by

$$\nabla \cdot \vec{q} = 0, \tag{1}$$

$$(\vec{q} \cdot \nabla)\vec{q} = -\frac{1}{\rho}\nabla p + \frac{\mu}{\rho}\nabla^2\vec{q} + \frac{1}{\rho}\vec{J} \times \vec{B}, \tag{2}$$

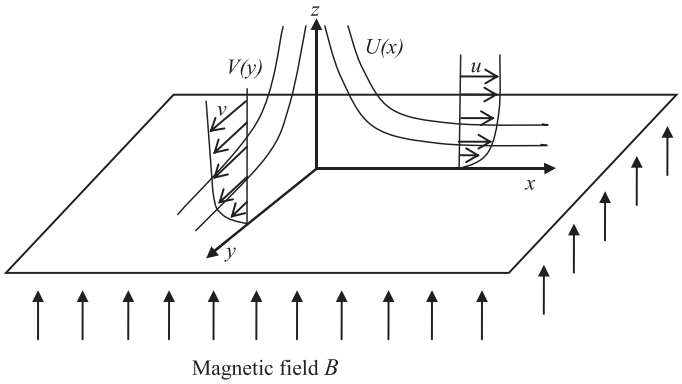


**Figure 1.** Physical configuration of the three-dimensional boundary-layer. The magnetic field $B$ is applied normal to the flow. The mainstream flows are denoted as $U(x)$ and $V(y)$.

where $\vec{q}$ is the velocity vector, $p$ is the pressure, $\mu$ is the dynamic viscosity, and $\vec{J}\times\vec{B}$ is body force that is coupled between the magnetic field and the fluid motion that is called Lorentz force. The induced magnetic field is assumed to be negligible because the magnetic Reynolds number is very small. This plays a vital role in some engineering problems where the conductivity is not large in the absence of an externally applied magnetic field. It has been taken that $E = 0$. Thus, from the Ohm's law, it is given by

$$\vec{J} = \vec{q}\times\vec{B}. \tag{3}$$

Taking the curl of the last term of (2) with the aforementioned equation, we obtain

$$\vec{J}\times\vec{B} = [-uB^2\hat{i} - vB^2\hat{j} + 0\cdot\hat{k}]. \tag{4}$$

Let $U(x)$ be the velocity along $x$-direction and $V(y)$ be the velocity along $y$-direction outside the boundary-layer (mainstream flow velocities). Because the Reynolds number is large, the viscosity effects are dominant adjacent to the wedge surface. If $\delta$ is the thickness of the boundary layer, then this estimates an order of magnitude of each term with $\delta \ll L$ where $L$ is the reference length of the surface. This clearly results into the other basic approximation $|\partial u/\partial x|, |\partial u/\partial y| \ll |\partial u/\partial z|$ and $|\partial v/\partial x|, |\partial v/\partial y| \ll |\partial v/\partial z|$. From these assumptions, the continuity and momentum equations are given by

$$\frac{\partial u}{\partial x} + \frac{\partial v}{\partial y} + \frac{\partial w}{\partial z} = 0, \tag{5}$$

$$u\frac{\partial u}{\partial x} + v\frac{\partial u}{\partial y} + w\frac{\partial u}{\partial z} = -\frac{1}{\rho}\frac{\partial p}{\partial x} + \nu\frac{\partial^2 u}{\partial z^2} - \frac{\sigma B^2}{\rho}u, \tag{6}$$

$$u\frac{\partial v}{\partial x} + v\frac{\partial v}{\partial y} + w\frac{\partial v}{\partial z} = -\frac{1}{\rho}\frac{\partial p}{\partial y} + \nu\frac{\partial^2 v}{\partial z^2} - \frac{\sigma B^2}{\rho}v, \tag{7}$$

$$0 = \frac{\partial p}{\partial z}. \tag{8}$$

Equation (8) shows that the pressure variation along the normal direction is constant throughout the flow field. This means that in the flow field, the pressure $p$ is a function of $x$ and $y$ only. Thus, from Bernoulli's equation, the pressure gradients are given by

$$U\frac{dU}{dx} = -\frac{1}{\rho}\frac{\partial p}{\partial x} - \frac{\sigma B^2}{\rho}U, \tag{9}$$

$$V\frac{dV}{dy} = -\frac{1}{\rho}\frac{\partial p}{\partial y} - \frac{\sigma B^2}{\rho}V. \tag{10}$$

Substituting (9) and (10) in (6) and (7), we obtain the MHD boundary layer equations as

$$\frac{\partial u}{\partial x} + \frac{\partial v}{\partial y} + \frac{\partial w}{\partial z} = 0, \tag{11a}$$

$$u\frac{\partial u}{\partial x} + v\frac{\partial u}{\partial y} + w\frac{\partial u}{\partial z} = U\frac{dU}{dx} + \nu\frac{\partial^2 u}{\partial z^2} - \frac{\sigma B^2}{\rho}(u - U), \tag{11b}$$

$$u\frac{\partial v}{\partial x} + v\frac{\partial v}{\partial y} + w\frac{\partial v}{\partial z} = V\frac{dV}{dy} + \nu\frac{\partial^2 v}{\partial z^2} - \frac{\sigma B^2}{\rho}(v - V). \tag{11c}$$

The first term in the right-hand side of the aforementioned equations have been derived from the inviscid theory in the mainstream. The relevant boundary conditions for the aforementioned model are

$$\begin{aligned} &\text{at } z = 0: \quad u = v = w = 0, \quad \text{and} \\ &\text{as } z \to \infty: \quad u \to U(x) \quad \text{and} \quad v \to V(y). \end{aligned} \tag{12}$$

Note that the velocity of the fluid on the surface is zero and varies in the direction normal to the flow and merges with mainstream flow far away from the surface. As stated before, it is quite challenging to solve the aforementioned system; we solve it by using suitable similarity transformations on the assumption that the similar velocity profiles exist in both directions of the flow. Substituting the following similarity transformations and the aforementioned scaling defined

$$u = (a+b)xf'(\eta), \quad v = (a-b)yg'(\eta), \quad w = -\sqrt{\frac{\nu}{a}}[(a+b)f(\eta) + (a-b)g(\eta)], \tag{13}$$

with $\eta = \sqrt{a/\nu}z$, into the system (11) and (12), we obtain coupled nonlinear ordinary differential equations:

$$f''' - (1+\lambda)(f'^2 - ff'' - 1) + (1-\lambda)gf'' - M^2(f'-1) = 0, \tag{14a}$$

$$g''' - (1-\lambda)(g'^2 - gg'' - 1) + (1+\lambda)fg'' - M^2(g'-1) = 0, \tag{14b}$$

with the boundary conditions

$$f(0) = g(0) = 0, \quad f'(0) = g'(0) = 0, \quad f'(+\infty) = g'(+\infty) = 1, \tag{15}$$

where $f = f(\eta)$, $g = g(\eta)$ and primes denote derivative with respect to $\eta$. System (14) consists of third-order coupled nonlinear differential equations, which describe the MHD three-dimensional boundary-layer stagnation point flow. Parameter $M\left(=\sqrt{\frac{\sigma}{\rho a}}B\right)$ is the magnetic (Hartman number) parameter, which is the ratio of electromagnetic force to the viscous force, and $\lambda(=b/a)$ is shear-to-strain-rate where $a$ is the strain rate and $b$ is the shear rate. In the absence of magnetic field ($M = 0$), Howarth [2] gave the solutions for various values of $\lambda$ between 0 and 1. Note that the solutions of the aforementioned system are exact solutions of the Navier–Stokes equations in the boundary-layer limit. We aim to establish the existence of similarity solutions in each parameter range and to determine flow structure in the boundary layer. It is worth to notice that system (14) exhibits the reflexive symmetries

$$f(\eta,\lambda,M) = g(\eta,-\lambda,M), \quad f(\eta,-\lambda,M) = g(\eta,\lambda,M) \tag{16}$$

in which the aforementioned ansatz agrees with Weidman [14] in the absence of magnetic field. The aforementioned system of nonlinear ordinary differential equations is solved numerically using Keller-box method that consists of several steps. The (third) order of each equation in the system (14) is reduced to (six) first-order equations by introducing extra unknown functions. The central differences are then used to discretize these first-order equations, wherein no derivatives are evaluated at $\eta_i$ and with derivatives are evaluated at $\eta_{i-\frac{1}{2}}$. This type of discretization allows to use a very fine grid in order to capture the significant variations in the flow (such as the reverse flows). This discretization of the aforementioned six equations produces the nonlinear system of algebraic equations, and these are solved by Newton's linearization. LU decomposition method is used to solve the block system for corrections. Tolerance of the method was set to $10^{-6}$, and different integration domains were tested to obtain the same convergent solutions. This aforementioned method has been used effectively to investigate various physical mechanisms for different values of $\lambda$ and $M$. Note that the quantitative accuracy can be obtained only for moderate values of $\lambda$ and $M$. We therefore pursue our analysis of (14) and (15) for large $\lambda$. Once the solutions have been obtained for a given magnetic field, the displacement thicknesses along $x$-axis and $y$-axes may be as

$$\int_0^\infty (1 - f'(\eta))d\eta = \xi_x, \qquad \int_0^\infty (1 - g'(\eta))d\eta = \xi_y. \tag{17}$$

Thus, numerical integrations have been included as a part of the calculations. It will be shown how the displacement thicknesses vary for both $\lambda$ and $M$, and these predictions shall be discussed later. We first examine below the system behavior for large $\lambda$.

In the next section, we study the asymptotic behavior of the three-dimensional boundary-layer flow problem for large $\lambda$ and large $\eta$. This asymptotic study is important for two reasons. Firstly, the Keller-box results are completely justifiable from the asymptotic results. When $\lambda$ is large enough, the Keller-box method suffers with a slow convergence. Therefore, it is advisable to resort to obtain the asymptotic solutions of the three-dimensional equations for large $\lambda$ so that the results with the same accuracy can be obtained. Secondly, on the other hand, the boundary conditions defined in (12) or (15) suggest that the velocity profiles behave linearly far-away from the wedge surface. Thus, it is interesting to analyze the far-field behavior of the model. These two cases give a good deal of simplifications in the full nonlinear system (14). This analysis is given in the succeeding discussion.

## 3. Asymptotic behavior

### 3.1. Asymptotic for $\lambda \to \infty$

When the shear-to-strain-rate parameter $\lambda$ is large enough, the Keller-box method for system (14) suffers a slow convergence and requires large flow domain to satisfy the derivative condition at infinity. Therefore, it is advisable to obtain the asymptotic behavior for large $\lambda$. Defining

$$f(\eta) = \frac{H_1(\zeta)}{\sqrt{\lambda}}, \quad g(\eta) = \frac{H_2(\zeta)}{\sqrt{\lambda}}, \quad M^2 = M^{*2}\lambda, \tag{18}$$

where $\zeta = \sqrt{\lambda}\eta$ and $\frac{1}{\lambda} \ll 1$. The derivatives of (18) are substituted in the system of equations (14) and (15); we obtain

$$H_1''' - (1 + 1/\lambda)(H_1'^2 - H_1H_1'' - 1) + (1/\lambda - 1)H_2H_1'' - M^{*2}(H_1' - 1) = 0, \tag{19a}$$

$$H_2''' - (1/\lambda - 1)(H_2'^2 - H_2H_2'' - 1) + (1/\lambda + 1)H_1H_2'' - M^{*2}(H_2' - 1) = 0, \tag{19b}$$

and the boundary conditions become

$$H_1(0) = H_2(0) = 0, \quad H_1'(0) = H_2'(0) = 0, \quad H_1'(\infty) = H_2'(\infty) = 1, \tag{20}$$

where primes now denote the derivative with respect to $\zeta$. System (19) contains a small parameter $(1/\lambda)$, and therefore, it is appropriate to use the regular perturbation method as

$$\begin{aligned} H_1(\zeta) &= H_{10}(\zeta) + (1/\lambda)\,H_{11}(\zeta) + \left(1/\lambda^2\right)H_{12}(\zeta) + \ldots \\ H_2(\zeta) &= H_{20}(\zeta) + (1/\lambda)\,H_{21}(\zeta) + \left(1/\lambda^2\right)H_{22}(\zeta) + \ldots \end{aligned} \tag{21}$$

in (19) and (20). The zeroth-order system is given by

$$H_{10}''' + H_{10}H_{10}'' - H_{10}'^2 + 1 - H_{20}H_{10}'' - M^{*2}(H_{10}' - 1) = 0, \tag{22a}$$

$$H_{20}''' - H_{20}H_{20}'' + H_{20}'^2 - 1 + H_{10}H_{20}'' - M^{*2}(H_{20}' - 1) = 0, \tag{22b}$$

with the boundary conditions

$$H_{10}(0) = H_{20}(0) = 0, \quad H_{10}'(0) = H_{20}'(0) = 0, \quad H_{10}'(\infty) = H_{20}'(\infty) = 1. \tag{23}$$

For $M^* = 0$, numerical solutions of the system (22) are given by Davey [16] and Weidman [14]. The aforementioned system of (22) with the boundary conditions (23) is solved again using the Keller-box method. The shear stresses for $\lambda \gg 1$ for different values of $M^*$ are given by

$$f''(0) = \sqrt{\lambda}H_{10}''(0), \qquad g''(0) = \sqrt{\lambda}H_{20}''(0). \tag{24}$$

Note from (24) that both shear stress parameters grow indefinitely for given $M^*$. The displacement thicknesses are obtained by

$$\frac{1}{\sqrt{\lambda}}\int_0^\infty (1 - H_{10}'(\zeta, M^*))d\zeta = \xi_{x0}, \qquad \frac{1}{\sqrt{\lambda}}\int_0^\infty (1 - H_{20}'(\zeta, M^*))d\zeta = \xi_{y0}. \tag{25}$$

The displacement thicknesses $\xi_{x0}$ and $\xi_{y0}$ are computed using the numerical integration and is part of our code.

### 3.2. Far-field behavior

In this section we analyze the far-field behavior of the governing equations. The derivative boundary conditions at edge of the boundary-layer suggest to analyze the local behavior of the solutions, that is, $|f'(\eta) - 1| \ll 1$ and $|g'(\eta) - 1| \ll 1$ as $\eta \to \infty$. This helps us to define new stream functions as

$$f(\eta) \sim \xi_x + \eta + F(\eta), \qquad g(\eta) \sim \xi_y + \eta + G(\eta), \tag{26}$$

where $F(\eta)$, $G(\eta)$ and their derivatives are assumed small. Substituting (26) with $f'(\eta) = 1 + F'(\eta) = 1 + F_1(\eta)$, $g'(\eta) = 1 + G'(\eta) = 1 + G_1(\eta)$, $f''(\eta) = F_1'(\eta)$, $g''(\eta) = G_1'(\eta)$, $f'''(\eta) = F_1''(\eta)$ and $g'''(\eta) = G_1''(\eta)$ into systems (14) and (15), and linearizing the resulting ordinary differential equations, we obtain another set of linear ordinary differential equations as

$$F_1'' + (\delta + \eta)F_1' - (2(1 + \lambda) + M^2)F_1 = 0, \tag{27a}$$

$$G_1'' + (\delta + \eta)G_1' - (2(1 - \lambda) + M^2)G_1 = 0, \tag{27b}$$

and boundary conditions take the form

$$F_1(0) = G_1(0) = -1, \quad F_1(\infty) = G_1(\infty) = 0, \tag{28}$$

where

$$\delta = \frac{(1+\lambda)\xi_x + (1-\lambda)\xi_y}{2} \tag{29}$$

is the three-dimensional displacement thickness at the point of attachment (Lighthill [17]; Davey [16]). It is clearly observed that system (27) also has the reflexive symmetries. Solutions of (27) are given by

$$F_1(\eta) = C_1(\eta+\delta)F\left(\frac{1}{2}+K_1, \frac{3}{2}, -(\eta+\delta)^2\right) + D_1F\left(K_1, \frac{1}{2}, -(\eta+\delta)^2\right), \tag{30a}$$

$$G_1(\eta) = C_2(\eta+\delta)F\left(\frac{1}{2}+K_2, \frac{3}{2}, -(\eta+\delta)^2\right) + D_2F\left(K_2, \frac{1}{2}, -(\eta+\delta)^2\right) \tag{30b}$$

where

$$C_N = W_N/A_N, \quad D_N = -1/A_N,$$

$A_N = -W_N\delta F\left(\frac{1}{2}+K_N, \frac{3}{2}, -\delta^2\right) + F\left(K_N, \frac{1}{2}, -\delta^2\right)$, $W_N = \frac{\Gamma(1-K_N)\Gamma(\frac{1}{2})}{\Gamma(\frac{1}{2}-K_N)\Gamma(\frac{3}{2})}$, $K_1 = \frac{-(2(1+\lambda)+M^2)}{4}$ and $K_2 = \frac{-(2(1-\lambda)+M^2)}{4}$, for $N = 1, 2$. Using the identity $F\left(\hat{a}, \hat{b}, z\right) = e^zF\left(\hat{b}-\hat{a}, \hat{b}, -z\right)$ (Abramowitz and Stegun [18]), solutions (30) become

$$F_1(\eta) = C_1Z^{\frac{1}{2}}e^{-Z}F\left(1-K_1, \frac{3}{2}, Z\right) + D_1e^{-Z}F\left(\frac{1}{2}-K_1, \frac{1}{2}, Z\right), \tag{31a}$$

$$G_1(\eta) = C_2Z^{\frac{1}{2}}e^{-Z}F\left(1-K_2, \frac{3}{2}, Z\right) + D_2e^{-Z}F\left(\frac{1}{2}-K_2, \frac{1}{2}, Z\right), \tag{31b}$$

where $Z = (\eta+\delta)^2$. For large $Z$ (i.e., as $\eta \to \infty$), (31) can be rewritten as

$$F_1(\eta) \sim Z^{(K_1-\frac{1}{2})}e^{-Z}\left(\frac{C_1e^{\pm i\pi(1-K_1)}\Gamma(\frac{3}{2})}{\Gamma(\frac{1}{2}+K_1)} + \frac{D_1e^{\pm i\pi(\frac{1}{2}-K_1)}\Gamma(\frac{1}{2})}{\Gamma(K_1)}\right) - Z^{-K_1}\left[\frac{C_1\Gamma(\frac{3}{2})}{\Gamma(1-K_1)} + \frac{D_1\Gamma(\frac{1}{2})}{\Gamma(\frac{1}{2}-K_1)}\right], \tag{32a}$$

$$G_1(\eta) \sim Z^{(K_2-\frac{1}{2})}e^{-Z}\left(\frac{C_2e^{\pm i\pi(1-K_2)}\Gamma(\frac{3}{2})}{\Gamma(\frac{1}{2}+K_2)} + \frac{D_2e^{\pm i\pi(\frac{1}{2}-K_2)}\Gamma(\frac{1}{2})}{\Gamma(K_2)}\right) - Z^{-K_2}\left[\frac{C_2\Gamma(\frac{3}{2})}{\Gamma(1-K_2)} + \frac{D_2\Gamma(\frac{1}{2})}{\Gamma(\frac{1}{2}-K_2)}\right]. \tag{32b}$$

Using appropriate constants defined in (3.2), the terms between square brackets in (32) become zero, and therefore from (32), we have

$$F_1(\eta) \sim Z^{(K_1-\frac{1}{2})}e^{-Z}\left(\frac{C_1e^{\pm i\pi(1-K_1)}\Gamma(\frac{3}{2})}{\Gamma(\frac{1}{2}+K_1)} + \frac{D_1e^{\pm i\pi(\frac{1}{2}-K_1)}\Gamma(\frac{1}{2})}{\Gamma(K_1)}\right), \tag{33a}$$

$$G_1(\eta) \sim Z^{(K_2-\frac{1}{2})}e^{-Z}\left(\frac{C_2e^{\pm i\pi(1-K_2)}\Gamma(\frac{3}{2})}{\Gamma(\frac{1}{2}+K_2)} + \frac{D_2e^{\pm i\pi(\frac{1}{2}-K_2)}\Gamma(\frac{1}{2})}{\Gamma(K_2)}\right), \tag{33b}$$

which means that the solutions (33) converge exponentially as $Z \to \infty$ (as $\eta \to \infty$) for given $\lambda$ and magnetic number $M$. Thus, these solutions with (26) decay monotonically as $\eta \to \infty$ but satisfy the free stream flow. Table I gives the values for the skin-frictions $f''(0)$ and $g''(0)$ obtained from the system (26) for various values of $\lambda$ and magnetic number $M$. It is seen that even the linearized system also obeys the reflexive symmetries for all values of the magnetic number $M$. This reflexive symmetry is such that for increasing $\lambda$, shear stress $f''(0)$ is found to be decreasing, whereas $g''(0)$ increases continuously. These results are in good agreement with the large $\lambda$ asymptotics, which shall be discussed later.

**Table I.** Skin friction $f''(0)$ and $g''(0)$ obtained by asymptotic solution (26) for different values of $\lambda$ and $M$.

| | $M=1$ | | $M=2$ | |
|---|---|---|---|---|
| $\lambda$ | $f''(0)$ | $g''(0)$ | $f''(0)$ | $g''(0)$ |
| −2.0 | 1.26396 | −0.44761 | 0.08156 | −1.55788 |
| −1.5 | 0.75795 | −1.25899 | −0.36148 | −1.77446 |
| −1.0 | 0.15094 | −1.28306 | −0.79343 | −1.78291 |
| −0.5 | −0.39858 | −1.11846 | −1.15986 | −1.66070 |
| 0 | −0.82362 | −0.82362 | −1.44933 | −1.44933 |
| 0.5 | −1.11846 | −0.39858 | −1.66070 | −1.15986 |
| 1.0 | −1.28306 | 0.15094 | −1.78291 | −0.79343 |
| 1.5 | −1.25899 | 0.75795 | −1.77446 | −0.36148 |
| 2.0 | −0.44761 | 1.26396 | −1.55788 | 0.08156 |

## 4. Results and discussion

The uniform shear flows $u = by$ and $v = bx$ in magnetic field are projected onto the outer potential flow $u = ax$, $v = ay$, and $w = -az$, which leads to a new family of stagnation point flow problem that is governed by two important parameters shear-to-strain-rate $\lambda$ and magnetic parameter $M$ and solution exists over the region $-\infty < \lambda < \infty$ and $M > 0$. This governing system has been solved by the standard Keller-box method that is second-order accurate. The error tolerance for the Keller-box method was set to $10^{-6}$ for simulations. Because the domain is infinite, but for numerical computation, the physical domain has to be finite. We therefore fix the value of $\eta$ at different values to achieve the same solutions. For large-enough $\lambda$, this method did not converge, or sometimes, convergence slows down for given magnetic field. In this range, the asymptotic expansions of the system of equations (14) for large $\lambda$ has been obtained via the regular perturbation. Ranges of parameter space have been chosen, which is according to the physical dynamics of the problem, and various effects are investigated through displacement thicknesses, velocity profiles, and shear stress values. Note that for zero-shear-to-strain-rate, flows in the two boundary-layers are then identical, that is, $f(\eta) \equiv g(\eta)$, and only one set of MHD boundary layer equations needs to be solved. The various results discussed are confined to the solutions that satisfy their end conditions ($f'(\infty) = 1 = g'(\infty)$) asymptotically. The similarity solutions, when they exist, are exact solutions of the Navier–Stokes equations in the boundary-layer limit.

Figure 2 displays the variation of the wall shear stresses $f''(0)$ and $g''(0)$ with $\lambda$ for different values of Hartmann number $M$, and these are shown by solid lines. These values have been obtained from the direct numerical solution of the system (14) for various values of $M$. It is observed that the wall shear stresses $f''(0)$ ($g''(0)$) increases (decreases) gradually for increasing $\lambda$. These values are larger for large values of $M$. Note clearly that these wall shear stresses exhibit the reflection symmetry given by equation (16), and this symmetry trend is preserved for all magnetic field $M$. For non-magnetic field ($M = 0$), the zero-shear-stress occurs at $\lambda = \pm 2.5056$ as obtained by Weidman [14]; for $M = 1$, it occurs at $\lambda = \pm 3.8564$, etc. These zero-shear-stresses have been marked with thick circles in this figure for all $M$. As magnetic parameter is increased, the occurrence of zero-shear-stress at $|\lambda|$ also increases, and system always keeps the reflection symmetry. Again, these results are further complemented by the large $\lambda$ asymptotic, which are shown by the dashed lines in the same figure.

Variation of two-dimensional displacement thicknesses $\xi_x$, $\xi_y$ and the three-dimensional displacement thickness $\delta$ with shear-to-strain-rate $\lambda$ are plotted in Figure 3 for various values of magnetic number $M$ along with the large $\lambda$ asymptotics. In Figure 3, the solid lines represent the displacement thicknesses that are obtained from the numerical solution of (17) and (29), while the dashed lines are obtained from the asymptotic solution of (25) and three-dimensional displacement thickness (29) with $\xi_x = \lambda^{1/2}\xi_{x0}$ and $\xi_y = \lambda^{1/2}\xi_{y0}$. The large $\lambda$ asymptotic results are rather remarkable for applied magnetic field. Note that two-dimensional displacement thicknesses are always positive for all $\lambda$. It is observed that $\xi_x$ ($\xi_y$) decreases (increases) monotonically for increasing $\lambda$. This typical trend is observed for all values of the magnetic parameter $M$. It is interesting to note that, in accordance with the velocity profiles, the effect of magnetic

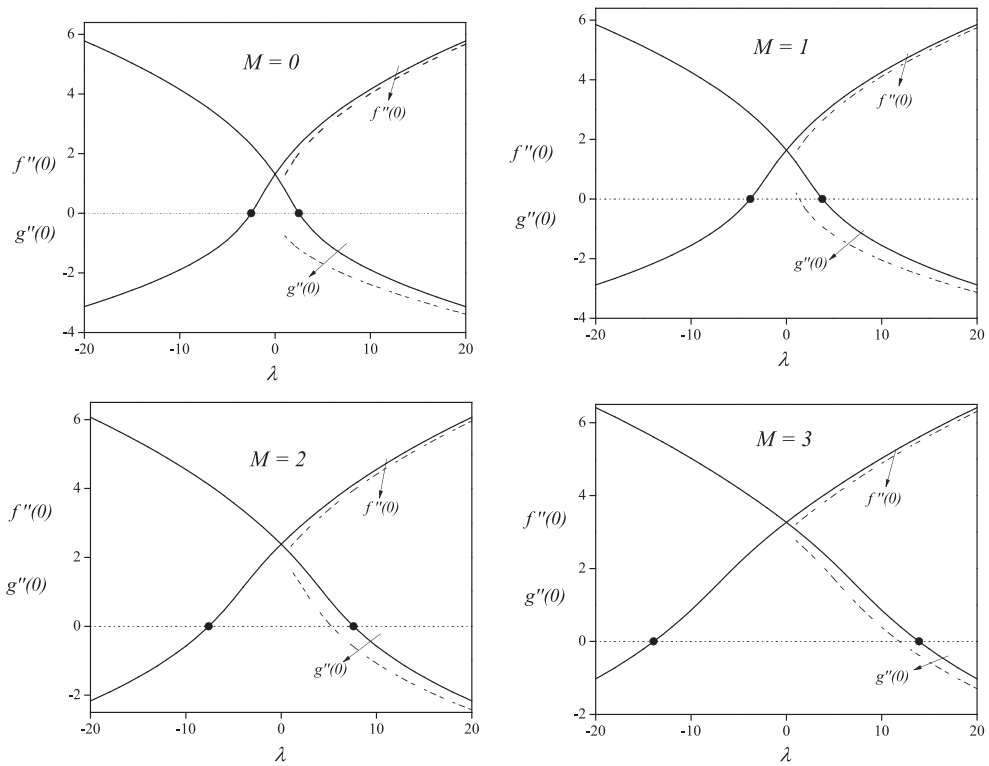


**Figure 2.** Illustration of how different shear stresses vary with $\lambda$ for different values of $M$. These are (solid lines) computed directly from the system (14) and (15), and dashed lines are from the asymptotic solution (24).

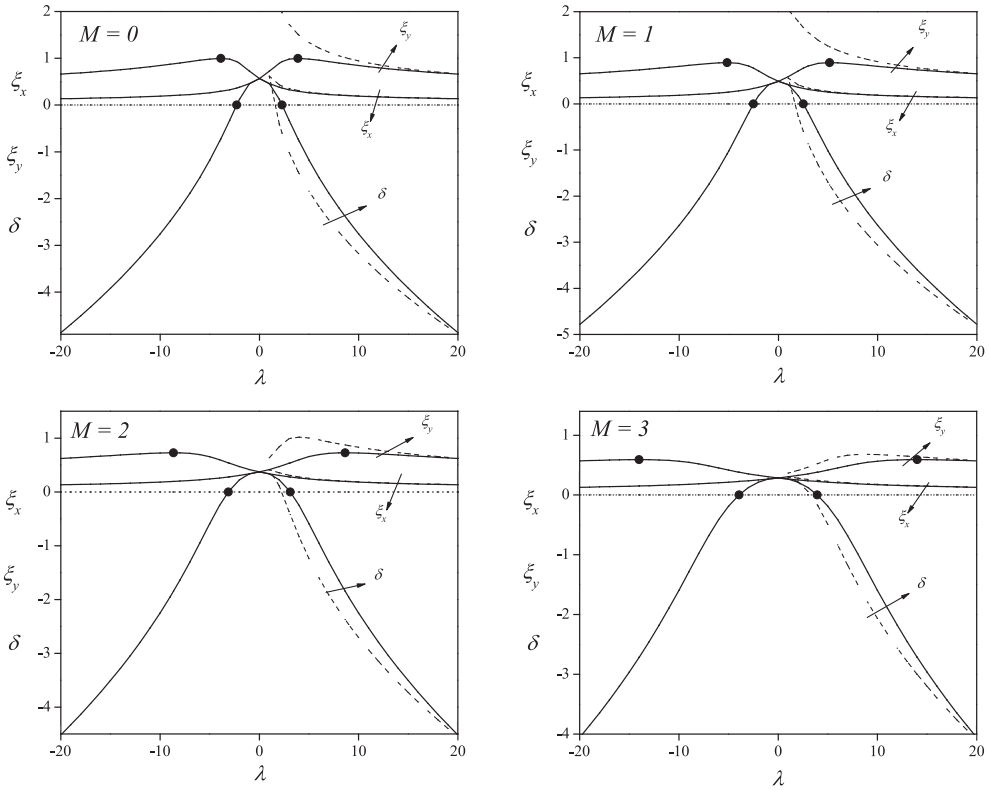


**Figure 3.** Computation of the displacement thicknesses (solid lines) directly from (25 and 29), and asymptotically (dashed) from (25 and 29 with $\xi_x = \xi_{x0}, \xi_y = \xi_{y0}$) for different values of $M$.

parameter $M$ is to decrease both the displacement thicknesses $\xi_x$ and $\xi_y$. This is because applied magnetic field decreases the boundary-layer thickness and hence the displacement thickness. Further, the three-dimensional displacement thickness $\delta$ first increases and achieves its positive maximum at $\lambda = 0$ and then starts decreasing as $\lambda$ increases from zero. These figures also show that the maximum values of displacement thicknesses are decreasing for increasing $M$. Note that as $|\lambda| \longrightarrow \infty$, three-dimensional thickness $\delta$ decreases unboundedly to negative infinity. Further evidence of this mechanism comes from the large asymptotic analysis that is given by (29), which shows that $\delta$ decreases to negative infinity.

Results of Figures 2 and 3 for various values of $M$ indicate that for $\lambda = 0$ the system becomes symmetric boundary layer, that is, $f(\eta) = g(\eta)$ for all $M$. Also, for $M = 0$ and $\lambda = 0$, the system reduces to Homann flow [12]. Further, for $\lambda = 0$ and $M \neq 0$ and because $f(\eta) = g(\eta)$, we need to solve one set of boundary layer equations (cf. (14)). We therefore intentionally simulated some of the velocity profiles for various magnetic field, and the profiles are presented in Figure 4(a). Note that the solid lines are for $f'(\eta)$, and lines with circles represent $g'(\eta)$. The results clearly indicate that for increasing magnetic field from $M = 0$ (Homann's flow), the thickness of the boundary-layer decreases. Further, Figure 4(b) describes the non-dimensional velocity profiles $f'(\eta)$ and $g'(\eta)$ as a function of $\eta$ for different values of $M$ and $\lambda = 1.5$. Note that the solid and dashed curves respectively represent $f'(\eta)$ and $g'(\eta)$. It is clearly observed that all the velocity profiles approach the outer potential flow condition asymptotically. The effect of magnetic field is to make the velocity curve to approach the outer boundary condition rapidly thereby steepening the boundary-layer thickness. These results are analogous to the MHD two-dimensional boundary-layer flow reported by Kudenatti *et al.* [19]. The momentum boundary-layer thickness decreases for increasing magnetic field. For increased magnetic field, the flow acquires more magnetization that leads to variation in Lorentz force that opposes the flow of the fluid. Therefore, the boundary-layer thickness decreases. The presence of magnetic field makes the three-dimensional boundary-layer flow rich both qualitatively and quantitatively. Next, the effect of shear-to strain-rate $\lambda$ further decreases the boundary-layer thickness.

In contrast to the aforementioned discussion, Figure 4(c) and (d) demonstrates the velocity profiles for different values of $\lambda$ for two values of $M$. Here, the thick line represents the results of $\lambda = 0$ for which the system becomes symmetric. Particularly, Figure 4(c) exhibits two distinct velocity profiles. Note that as discussed earlier, if $\lambda$ is further increased, the velocity profiles $f'(\eta)$ approach the potential flow very rapidly, while velocity profiles $g'(\eta)$ approach slowly. For some $\lambda$, profiles of $g'(\eta)$ show a reverse flow for small $\eta$ that contribute to the flow towards the surface, and then, flow is reattached. This flow reversal opposes the spread of vorticity away from the surfaces. These results are again complimented by large $\lambda$ asymptotics (Figure 4(f)). Nevertheless, when magnetic field is applied, these reverse flows disappear making an accelerated boundary-layer flow. Note that both velocity profiles ($f'(\eta)$, and $g'(\eta)$) approach their end condition very rapidly compared with non-magnetic field, thereby reducing the boundary-layer thickness.

Numerical solutions of (22) subject to (23), which represent that the velocity profiles for large $\lambda$ are given in Figure 4(e) and (f)

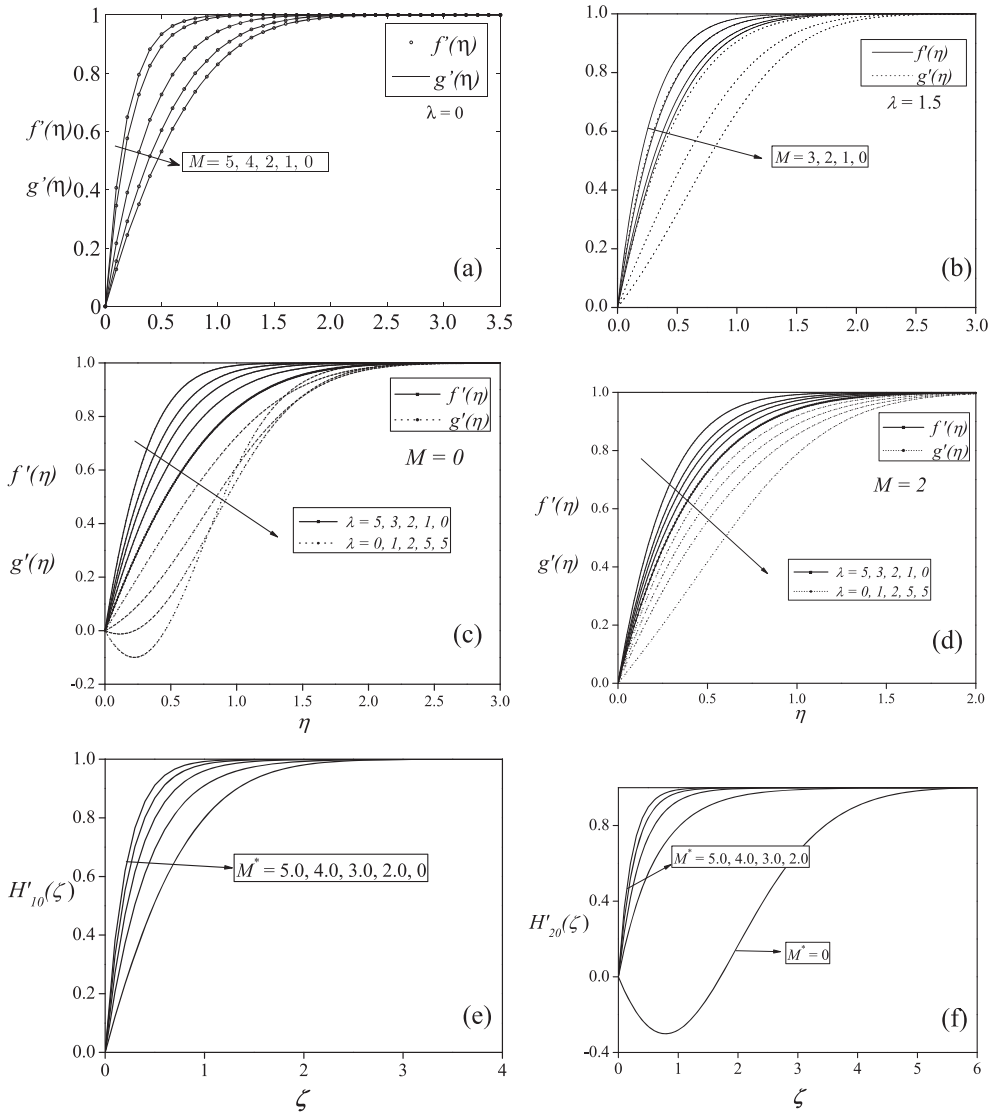


**Figure 4.** Variation of velocity profiles (direct and asymptotic, (e) and (f)) with $\eta$ ($\xi$) for different values of $\lambda$ and $M$ ($M^*$). These simulations have been performed using equations (14, 15), (22, and 23), and Keller-box method has been used in both cases.

for different values of $M^*$. These figures clearly show the effect of magnetic field that minimizes the boundary-layer thickness, and all velocity profiles are merging asymptotically with the outer mainstream flow. When $M^* = 0$, the reverse-flow is observed in $v$-component of flow, but eventually, it satisfies the end condition.

## 5. Conclusions

In this paper, the analyses have been carried out on the three-dimensional MHD flow of a viscous and incompressible fluid over a wedge in the presence of uniform magnetic field. The velocity field develops because of the interaction of magnetic field and the fluid in the boundary layer and also because of the mainstream flow. The governing equations have been solved numerically using the Keller-box method and by two asymptotic methods, and the solutions are interpreted for various parameters. Numerical computations are further complimented by the asymptotic solutions. The results have shown that the boundary-layer region is clearly divided into near-field and far-field regions. In the near-field, where viscosity effects are dominant, the streamwise velocity profiles reduce in both directions for increasing magnetic number $M$ and $\alpha$. This means that the flow field roughly divides into a near field where the viscosity modified by the magnetic force is important, and far-field region where inviscid flow plays a dominant role, for any combination of physical parameters. It is also observed that in the absence of magnetic field, there is a reverse flow in the $y$-momentum, which is not seen when we apply magnetic field. All these results are further and convincingly supported by an asymptotic study on the three-dimensional boundary-layer flow.

## Acknowledgements

The author RBK is grateful to the University Grants Commission (UGC), New Delhi, India for providing the financial support under the major research project (grant no. 39-32/2010 (SR)) to carry out this work. Authors thank the referees for their useful comments.

## References

1. Timman R. *A Calculation Method for Three-dimensional Laminar Boundary Layers*. National Luchtvaart lab. Amsterdam Rep. F., 1952,66.
2. Howarth L. Note on the boundary layers on a rotating sphere. *Philosophical Magazine and Journal of Science* 1951; **42**:1308–1315.
3. Sears WR. The boundary layer of yawed cylinders. *Journal of the Aeronautical Sciences* 1951; **16**:41–45.
4. Carrier GF. The boundary layer in a corner. *Quarterly of Applied Mathematics* 1947; **4**:367–370.
5. Blottner FG, Ellis MA. Finite difference solution of the incompressible three-dimensional boundary layer equations for blunt body. *Computers & Fluids* 1973; **1**:133–58.
6. Nickel K, Kirchgssner K. The Crocco transformation for the three-dimensional Prandtl boundary layer equations. *Mathematical Methods in the Applied Sciences* 1979; **1**:445–452.
7. Cousteix J. Three-dimensional and unsteady boundary layer computations. *Annual Review of Fluid Mechanics* 1986; **18**:173–196.
8. Kudenatti RB, Kirsur SR, Achala LN, Bujurke NM. Exact solution of two-dimensional MHD boundary layer flow over a semi-infinite flat plate. *Communications in Nonlinear Science and Numerical Simulation* 2013; **18**:1151–1161.
9. Takhar HS, Chamkha AJ, Nath G. Unsteady three dimensional MHD boundary layer ow due to the impulsive motion of a stretching surface. *Acta Mechanica* 2001; **146**:59–71.
10. Borelli A, Giantesio G, Patria MC. Numerical simulations of three-dimensional MHD stagnation point flow of a micropolar fluid. *Computers & Mathematics with Applications* 2013; **66**:472–489.
11. Abdou MA, Soliman AA. New explicit approximate solution of MHD viscoelastic boundary layer flow over stretching sheet. *Mathematical Methods in the Applied Sciences* 2012; **35**:1117–1125.
12. Homann F. Der Einfluss grosser Zahigkeit bei Stromung um Zylinder. *ZAMP* 1936; **16**:153–164.
13. Hewitt RE, Duck PW, Foster MR. Steady boundary-layer solutions for a swirling stratified fluid in a rotating cone. *Journal of Fluid Mechanics*; **384**: 339–374.
14. Weidman PD. Non-axisymmetric Homann stagnation-point flows. *Journal of Fluid Mechanics* 2012; **702**:460–469.
15. Rosenhead L. *Laminar Boundary Layers*. Clarendon Press: Oxford [England], 1963.
16. Davey A. Boundary layer flow at a saddle point of attachment. *Journal of Fluid Mechanics* 1961; **10**:593–610.
17. Lighthill MJ. On displacement thickness. *Journal of Fluid Mechanics* 1958; **4**:383–392.
18. Abramowitz M, Stegun I. *Handbook of Mathematical Functions*. Dover Publications: New York, 1970.
19. Kudenatti RB, Kirsur SR, Achala LN, Bujurke NM. MHD boundary layer ow over a non-linear stretching boundary with suction and injection. *International Journal of Non-Linear Mechanics* 2013; **50**:58–67.